JOM
https://doi.org/10.1007/s11837-018-2997-7

Modeling Argon Gas Behavior in Continuous Casting of Steel

HYUNJIN YANG,[1,3] SURYA P. VANKA,[1,4] and BRIAN G. THOMAS[2,5]

1.—Department of Mechanical Science and Engineering, University of Illinois at Urbana-Champaign, 1206 W. Green Street, Urbana, IL 61801, USA. 2.—Department of Mechanical Engineering, Colorado School of Mines, Brown Hall W370-B, 1610 Illinois Street, Golden, CO 80401, USA. 3.—e-mail: hyang69@illinois.edu. 4.—e-mail: spvanka@illinois.edu. 5.—e-mail: bgthomas@mines.edu

In the continuous casting of steel, argon gas injection through the upper tundish nozzle wall or stopper tip is known to decrease clogging and remove inclusions. In addition to this intended gas injection, gas may be passively aspirated into the flow system by negative pressure developed inside of the nozzle. The injected gas forms gas pockets and bubbles through complex redistribution processes that greatly affect flow in the mold, leading to defects in the final product. Estimating the number and size distribution of bubbles is crucial to optimize multiphase flow in this important manufacturing process. This article introduces an integrated methodology to investigate these phenomena and provides examples to validate the approach. The system features models to predict: gas leakage, pressure distribution in the entire system, gas pockets and the size distribution and trajectories of bubbles using a new hybrid method, and multiphase flow in the nozzle and mold.

INTRODUCTION

Argon gas is often injected during continuous casting of steel to lessen nozzle clogging.[1,2] It also greatly changes the flow pattern in the mold. If the bubbles are able to escape into the mold slag at the mold top, while not causing excessive level fluctuations and surface defects, then their net effect is beneficial for product quality. An additional benefit is that those escaping bubbles can help to remove detrimental inclusions from the system by attaching them to their surface.[3] Argon gas can reduce air aspiration problems by filling the low-pressure regions in the nozzle.[2] Unfortunately, argon gas injection can lead to serious defects in the final product if the bubbles cause detrimental flow instabilities in the mold or if they are entrapped into the final product.

Gas injection makes the continuous casting process difficult to control because of its complex nature and lack of a reliable methodology to analyze and understand its behavior. First, estimating the exact amount of gas in the flow system is challenging. The injected argon flow rate entering into the molten steel is often less than measured because of leakage[4] or is greater because of passive aspiration, as gas is sometimes supplied to feed into negative pressure regions, such as through joints in the slide gate. Another difficult problem is finding the evolving bubble size distribution, starting with the injected bubble size exiting from the UTN wall or stopper tip.

Second, the evolution and redistribution of gas bubbles within the highly turbulent flow inside the complex nozzle geometry are extremely complicated. Recent work[5] visualized the complex gas redistribution process and evolution of argon bubbles in a laboratory-scale stopper rod-like system, including phenomena such as the formation of gas pockets within the recirculation zones where bubbles can accumulate, the detachment of small bubbles from these large gas pockets by a complex shearing-off process, bubble interactions including coalescence and breakup, and volumetric expansion of the bubbles. Through those complex gas redistribution processes, the injected argon gas from the stopper tip or UTN porous wall is distributed into bubbles, which enter into the mold cavity with a certain bubble size distribution.

Third, the effect of bubbles on flow in the mold involves many complex phenomena. The buoyancy of the bubbles changes the fluid flow pattern in the mold according to their number and size distribution[6] and may cause flow instabilities, which triggers defect mechanisms such as slag entrainment, especially when they occur at the top surface.[7] The

Published online: 09 July 2018

bubble size distribution changes with position and time, in part because of differences in residence times of different bubble sizes.[8]

Finally, some bubbles may become captured into the dendritic interface of the solidifying steel shell, especially near the meniscus where hooks serve as a barrier to upward flow,[8] leading to both surface and internal defects.[9] Even though the fate of bubbles and their effect on the fluid flow are strongly related to their amount and size, previous work on multiphase mold flow in the mold has typically neglected many of the above phenomena. In this article, a new methodology is proposed to improve the prediction of multiphase flow in continuous casting with argon gas injection by integrating together several models developed by the authors in recent work, which address each of the four phenomena described above.

MODEL 1. GAS INJECTION THROUGH POROUS NOZZLE WALLS

The first component of the new methodology is to quantify where and how argon gas is delivered into the molten-steel flow system. The argon gas flow rate is usually calculated based on a measurement made at standard temperature and pressure far away from where it is injected into the nozzle, typically through porous refractory or passive aspiration. However, some of this gas may leak away before it enters the nozzle,[4] and the wide range of the pressure distribution inside the nozzle greatly affects the location and extent of gas expansion when the gas enters into the flow. Combined with the great volumetric thermal expansion of the gas due to the temperature increase from ambient to entering the molten steel, this makes prediction of the location and amount of gas during its initial injection very challenging.

To address these issues, a three-dimensional model of porous flow through the nozzle refractory has been developed to estimate the real gas flow rate entering into the flow system.[4] This model considers the effect of the non-uniform pressure and temperature, geometry and joint sealing conditions and features a one-way flow pressure boundary condition on porous refractory walls of the Upper Tundish Nozzle (UTN). This model calculates the gas velocity and pressure distribution within the porous wall. Gas bubbles form to enter the steel flow only where the pressure is sufficient to overcome the surface tension forces at the active sites in the permeable refractory. Because the plant typically measures both the gas flow rate and the back pressure at the nozzle, the redundant information can be used to calibrate the model to predict the extent of gas leakage.[4]

Next, a semi-empirical analytical model of gas injection into downward flowing liquid is applied to predict the average gas bubble size entering the nozzle. Experiments involving horizontal air injection into a nozzle with turbulent downward flowing water with high-speed videos were analyzed to develop a two-step analytical model to predict the average initial size of gas bubbles when injecting through a small opening into downward flowing liquid.[10] The model matches well with measurements in air–water systems[10,11] and can be extrapolated to the steel-argon system of interest to estimate the initial argon bubble size from the porous UTN wall.

Next, a simple empirical equation is applied to estimate the number of small openings, or "active sites," through which gas flows when injecting through porous refractory. Experiments[12] studied the behavior of air injection through porous refractory into turbulent downward flowing water. The refractory was coated with a very thin layer of wax-like material to decrease the wettability of the air–water system to better match with an argon-steel system. A correlation was developed to predict the number of active sites per unit surface area as a function of gas flow rate, average liquid velocity, the permeability of the porous material and contact angle.[12] Combined with the total gas flow rate and injection area from the porous flow model, and the downward steel velocity from a model of fluid flow in the nozzle, the number of active sites per unit area can be used to provide the number of active pores and the flow rate through each pore, which is needed for the two-step analytical model to predict the average bubble size.

The final sub-model is to extrapolate the average bubble size to a complete size distribution. This can be done using a Rosin–Rammler distribution, which has been shown to match reasonably well with measurements of entrapped bubble size distributions in as-cast slabs at Baosteel.[13] By combining these four submodels together, it is possible to estimate the initial argon bubble size distribution entering into the nozzle from the UTN porous wall.[14]

MODEL 2. PASSIVE ARGON GAS INJECTION (ASPIRATION)

The second part of this methodology is to predict the pressure distribution in the entire system and the extent of air aspiration into low-pressure regions just below the slide gate or stopper rod. The slide gate or stopper rod flow control causes a great pressure drop, which regulates the system flow rate. When a region with negative gage pressure (below atmospheric pressure) forms in the nozzle because of this pressure drop, gas may be drawn into the nozzle through any gaps or cracks. The oxygen in this air then reacts with the most reactive alloys, such as Al, Ca, or Si, to create non-metallic oxides in the steel. To avoid this scenario, argon gas is often provided to be sucked in passively instead of air.

A mathematical model has been developed to estimate the pressure distribution in the flow system, including these important negative pressure regions, based on solving a system of 1D pressure-energy equations.[15] Boundary conditions are atmospheric pressure at the top surfaces of the tundish and mold. Then, from the pressure difference between the inside and outside of the negative pressure region, the flow rate of this passively injected gas entering the system can be calculated.

As an example, Fig. 1 shows the gas volume fraction field in the nozzle calculated by the Eulerian–Eulerian (EE) model described in the next section, and Fig. 2 shows the pressure distribution calculated from the 1D pressure energy model. The new 1D pressure-energy model is observed to agree with the results from the computationally intensive EE model. Using the simple model to estimate the passive gas flow rate avoids the complexity and expense of a fully two-way coupled model system. In addition, this simple model can serve as a practical stand-alone tool that can be used for other purposes, such as the provision of pressure boundary conditions for other models that do not include the entire flow system.

In the example given in Figs. 1 and 2, both models predict significant negative pressure below the slide gate. Considering that the grooves in the slide gate plates were supplied with argon gas to avoid air aspiration, these joints will allow passive flow of argon gas into the low-pressure region below the slide gate. If leaks are excessive or if argon flow is insufficient, re-oxidation and nozzle clogging could occur. The argon flow rate needed to sustain positive pressure inside the nozzle (above 1 atm.) or casting condition changes that could avoid negative pressure generation can be predicted with this model.

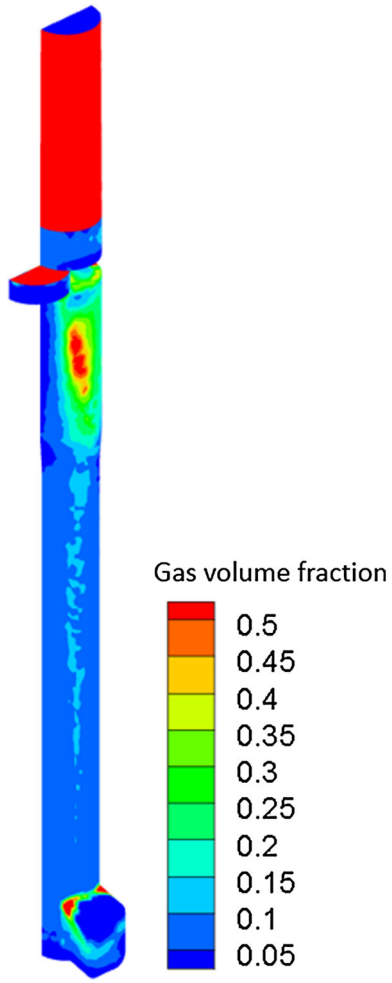

Fig. 1. Gas volume fraction in a slide gate nozzle.[15]

MODEL 3. REDISTRIBUTION AND EVOLUTION OF GAS BUBBLES IN THE NOZZLE

The third part of the methodology is to predict the complex multiphase flow behavior and size distribution of the argon gas pockets and bubbles in the nozzle flow. Once the total gas flow rate and size distribution of the injected gas bubbles has been calculated in the previous two steps, the next step is to estimate how these bubbles behave in the nozzle, as they interact with other gas pockets, bubbles, and molten steel flow in the nozzle and mold regions. The distribution of gas into bubbly flow or slug flow (with intermittent large gas-filled regions) is a highly challenging modeling task, as mentioned in the introduction, and only a few previous studies exist. The relevant phenomena occuring in the continuous-casting system can be organized as follows: (1) generation of recirculation zones by flow separation, (2) formation of gas pockets by the accumulation of bubbles within the recirculation zones, (3) bubble detachment from the gas pocket by shearing-off processes, and (4) bubble interactions (coalescence and breakup).

To simulate the above complex gas redistribution processes in an integrated manner and to estimate the evolution of the locally and time-varying bubble size distribution, a new multiphase flow model Eulerian–Eulerian Discrete-Phase Model (EEDPM) has recently been proposed.[15–17] As the name of the model suggests, the governing equations are composed of two parts: a Eulerian–Eulerian (EE) model calculates the velocity and volume fraction fields of each phase with a shared pressure field[18] from continuity and Navier–Stokes equations for each phase.

$$\frac{\partial(\alpha_k \rho_k)}{\partial t} + \nabla \cdot (\alpha_k \rho_k \boldsymbol{u}_k) = 0, \tag{1}$$

$$\frac{\partial(\alpha_k \rho_k \boldsymbol{u}_k)}{\partial t} + \nabla \cdot (\alpha_k \rho_k \boldsymbol{u}_k \boldsymbol{u}_k) = -\alpha_k \nabla p + \nabla \cdot \left(\mu_k \alpha_k \left(\nabla \boldsymbol{u}_k + \nabla \boldsymbol{u}_k^T\right)\right) + \alpha_k \rho_k \boldsymbol{g} + \boldsymbol{F_D}. \tag{2}$$

A DPM model tracks each bubble as a point mass, calculating the position and velocity of each bubble.[19]

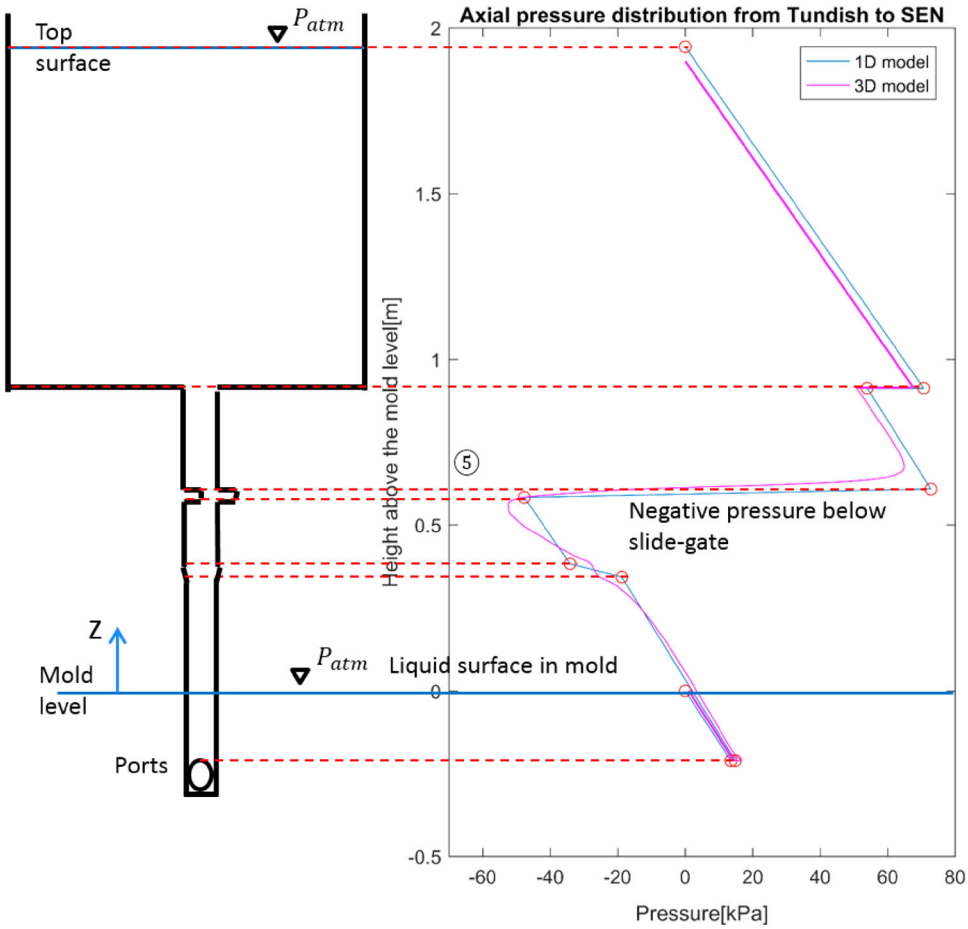

Fig. 2. Pressure distribution down the nozzle, comparing numerical and analytical models.[15]

$$\rho_g V_p \frac{\mathrm{d}\boldsymbol{v_i}}{\mathrm{d}t} = V_c(\boldsymbol{F_D} + \boldsymbol{F_V} + \boldsymbol{F_P} + \boldsymbol{F_B}), \tag{3}$$

$$\frac{\mathrm{d}\boldsymbol{x_i}}{\mathrm{d}t} = \boldsymbol{v_i}. \tag{4}$$

These two models are run together as separate models, with separate sets of momentum and mass conservation equations being solved simultaneously in the same domain. They are coupled together in several ways: the DPM momentum terms (RHS of Eq. 3) depend on the flow field from the EE model. Important forces governing the interaction between the gas bubbles and fluid are considered, including the drag, virtual mass, pressure gradient, and buoyancy forces.[20] The DPM bubble size also evolves transiently by bubble interactions (coalescence and breakup) and volumetric expansion of the bubbles according to the local pressure. At the same time, the instantaneous, spatially varying DPM bubble size distribution is given to the EE model, where it influences the drag force $\boldsymbol{F_D}$ between the gas and liquid phases in the EE model. Here, the Tomiyama drag force model is used for the drag.[21] Details of these models are discussed elsewhere.[15] As the EE liquid phase flow field is changed by the drag force based on the DPM bubble size, this model system is two-way coupled. Consequently, this hybrid model can predict the spatially and time-varying bubble size distributions, in addition to realistic formation and movement of large gas pockets. Mass conservation problems are avoided because no mass is exchanged between the two models. The location of gas pockets is obtained from the volume fraction field calculated by the EE model. The shearing-off process is estimated by applying the boundary layer theory and breakup models to the edges of the large gas pocket regions, which generates new DPM bubbles. The size, number, and position of these detached bubbles are calculated and input to the DPM model. At the same time, a coalescence model calculates the merging of individual bubbles into larger bubbles or gas pockets, and a breakup model captures breakup of bubbles according to the local level of turbulent fluctuations. The DPM model also tracks the evolving size of each bubble due volumetric expansion and contraction, which accompany the local temperature and pressure.

The components of this new EEDPM model are being validated by comparison with a variety of test problems where experimental measurements could

be found. The volumetric expansion model and the drag force model (Tomiyama drag) have been validated in a test problem involving a single bubble rising in stagnant water.[15] As the bubble expands as it rises because of the decrease of surrounding hydrostatic pressure, the bubble size and terminal velocity continuously vary. Figure 3 shows a comparison of the calculated terminal velocity of the bubble to previous works. The EEDPM model simulation matches reasonably well with flow in ultra-clean water.

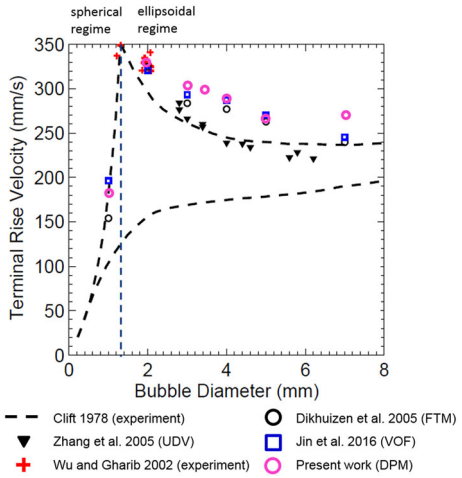

Fig. 3. Comparison of terminal velocities with previous works.[22]

A second test problem of upward bubbly flow in a vertical pipe is being used to evaluate the accuracy of the bubble interaction (coalescence and breakup) models.[15,20] Several test conditions, including both bubbly flow and transition-flow regimes, have been benchmarked. The EEDPM model results of velocity profiles, gas volume fraction, and radial bubble size distributions (Fig. 4) match reasonably well with the experimental measurements.

Third, the shearing-off model is being validated by comparing predictions of the shape of gas pockets in the nozzle and the bubble size distribution in the mold of a laboratory-scale stopper-rod-like system involving molten metal and argon gas flow[15,17] with measurements.[5] The combined effects of all of the components of the bubble models (gas pockets, volumetric expansion, coalescence, breakup, and shearing off) are tested together via test cases with this complex gas redistribution and flow system.

Figure 5 shows a comparison of predicted and measured gas pocket formation near the stopper rod tip, illustrating the gas-rich recirculation zones that form through the accumulation of argon gas injected from the stopper tip and the continuous detachment and coalescence processes involving small bubbles. A total of three gas pockets are formed at the

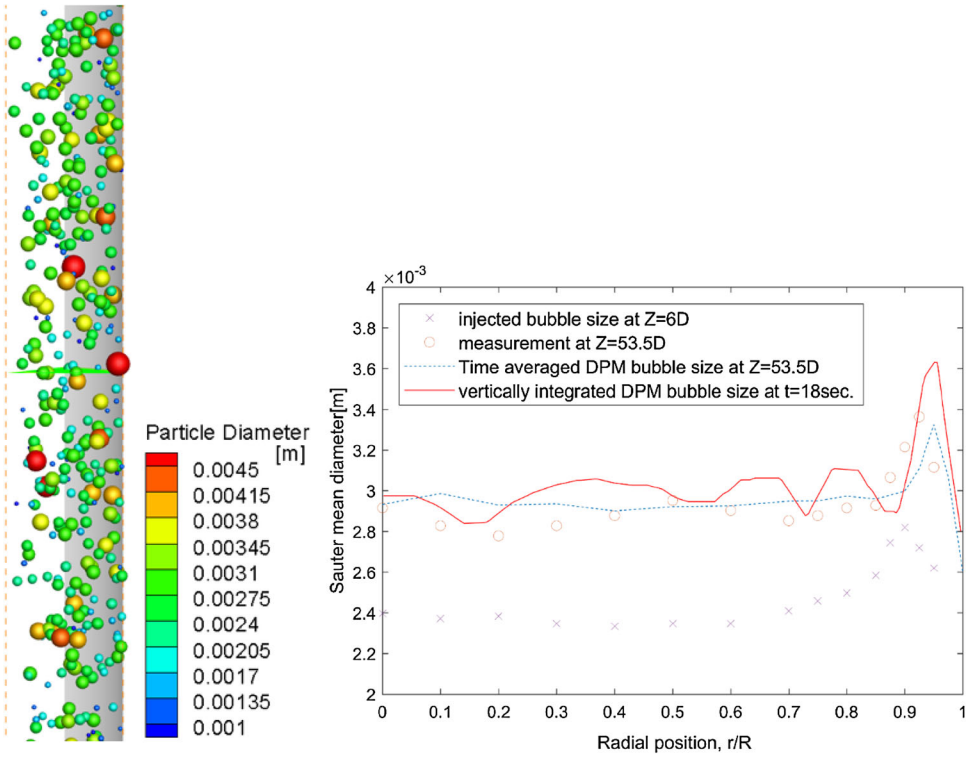

Fig. 4. EEDPM simulation of upward bubbly flow and comparison of predicted bubble size distribution with measurements. Reprinted with permission from Ref. 20.

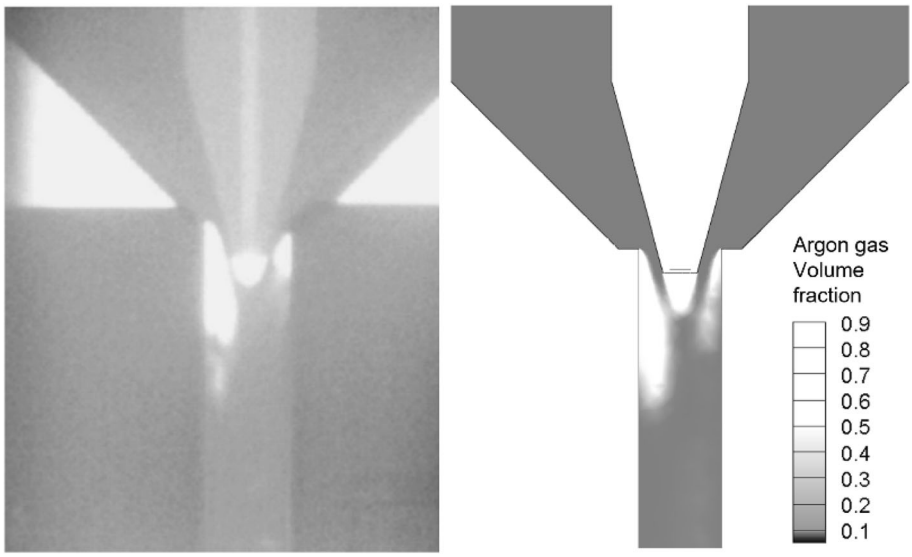

Fig. 5. Sheared-off DPM bubbles from gas pockets.

stopper tip and side walls of the nozzle near the inlet in both the measurement (Fig. 5a) and simulation (Fig. 5b). The shearing off of side gas pockets is observed sporadically in both results but is more periodic in the simulation than in the measurement video, where flow instabilities caused the gas pocket on the left side to remain larger for long time periods. The detached small bubbles flow down the nozzle toward the ports as a bubbly flow, and this process is captured with the shearing-off model in the DPM part of the simulation.

Figure 6 displays sample results of the sheared DPM bubbles size distribution and flow field. Due to the very thin mold of the laboratory test apparatus, the jets from the nozzle ports obstruct most of the bubbles from rising to the top once the bubbles flow into the lower mold. Bubbles circulate in the lower roll and experience coalescence and break up repeatedly. Relatively large bubbles (diameter $>$ 7 mm) evolve because of this serial coalescence phenomenon and are able to overcome the jet obstruction and float toward the top sporadically. Also, a high turbulence dissipation rate is observed near the bottom of the ports with the development of swirl, which causes breakup of the largest bubbles (diameter $>$ 6 mm) when they pass through the ports. Also, two relatively large bubbles are observed staying at the top of each port because of the coalescence of DPM bubbles, which are able to accumulate within the recirculation zones in this region of the nozzle, owing to its downward-directed ports.

Figure 7 compares the calculated bubble size distribution with the experimental measurement.[5] The calculation results show reasonable agreement. The majority of bubbles have diameter = 1–3 mm because the average turbulence dissipation rate in the nozzle ($\varepsilon = 1-10\,\mathrm{m}^2/\mathrm{s}^3$) allows maximum stable bubble sizes in this range.

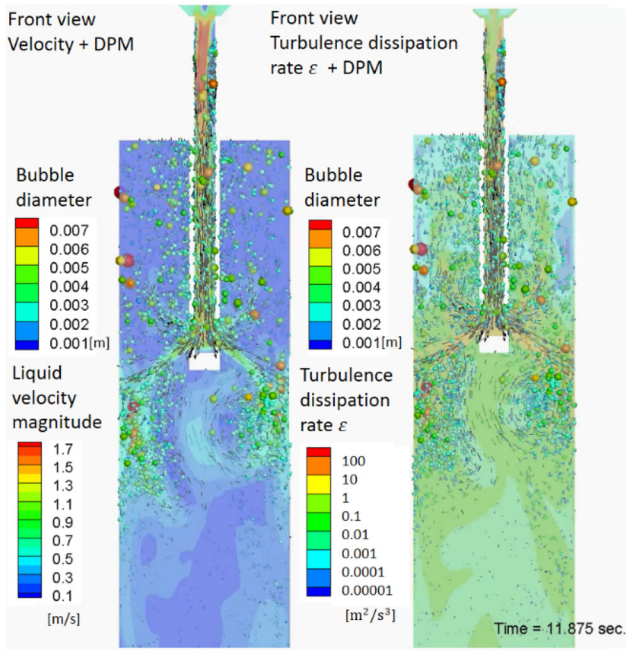

Fig. 6. DPM bubble distribution with fields of velocity (left) and turbulence dissipation rate (right). Reprinted without permission from Ref. 17.

This validated EEDPM is next applied to a full-scale slide gate nozzle with realistic geometry. Figure 8 shows an example of the bubbles and gas pockets distributed within the region just below the sliding plate in a typical continuous-casting operation. It is important to note that gas pocket formation is not always predicted, because it depends on the casting conditions and nozzle geometry. In this case, gas pockets (red zone in the Fig. 8) are predicted to form just below the slide gate system and at the top of the port, as expected because of the

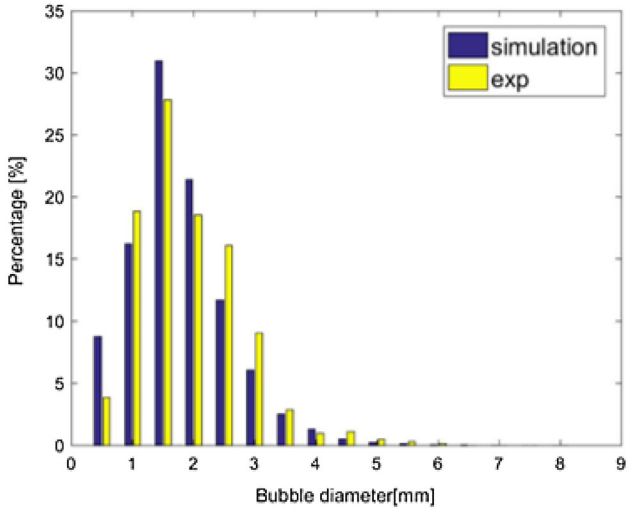

Fig. 7. Bubble size distribution in the lower mold, comparing predictions and measurements. Reprinted without permission from Ref. 17.

gas accumulation inside the recirculation zones. Relatively larger bubbles are observed in recirculation regions not filled by gas pockets because of the coalescence effect. It is important to note that the initial bubble size distribution is much more important to the final bubble size in such realistic commercial continuous-casting nozzles than it is in the laboratory flow system of the third test problem, discussed in Figs. 5, 6 and 7 above.

MODEL 4. FLUID FLOW IN THE MOLD AND BUBBLE CAPTURE

The final stage of the methodology is the simulation of multiphase turbulent flow in the mold. The quality of the final steel product is directly related to this flow pattern through several defect mechanisms.[7] Numerous studies have been implemented to investigate multiphase flow in the continuous steel casting process, including the effects of bubbles,[6,23,24] magneto-hydrodynamics (MHD),[25–31] and casting geometry[32,33] on the flow pattern and top surface stability. However, these works simplify the bubble size distribution to a constant or to number of pre-fixed size distributions. Thus, the models in these previous works could be improved using the realistic bubble size distributions estimated with the methodology presented in the three previous sections, especially including the EEDPM model.

Another issue that can benefit from the new modeling approach is the simulation of bubble capture into the solidifying shell. Several previous studies were made to predict the capture of bubbles and inclusion particles during continuous casting.[13,34–39] An advanced capture criterion was developed in previous work that considers the local forces acting on a bubble when it contacts the dendrite tips.[13] Bubbles smaller than the Primary

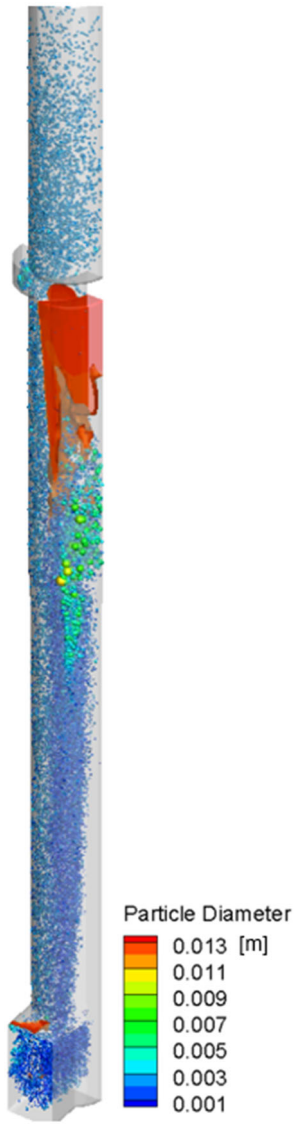

Fig. 8. Distributed argon gas bubbles and gas pocket in a real slide gate and nozzle operation.

Dendrite Arm Spacing (PDAS) are entrapped whenever they touch the solidified shell, but bubbles larger than the PDAS are captured when the vector sum of all of the local forces is able to reach a balance. In addition, hook formation enables another bubble capture mechanism near the meniscus by trapping rising bubbles beneath the partially solidified meniscus, which protrudes from the upper portion of the downward-moving steel shell like a hook.[40] The bubble size is a crucial component of these capture criteria to decide the fate of bubbles (escape to the top of the mold, capture by hooks near the meniscus or capture by the dendrites deep in the caster) for several reasons. First, the trajectory of each bubble is strongly affected by its size. Also, the bubble size changes the forces in the capture criterion. Furthermore, this is complicated because

the bubble size distribution in the mold varies locally owing to transport effects and differences in removal rate and consequently on the residence time.[8] Future studies of bubble capture can produce more realistic predictions by incorporating more accurate bubble size distributions based on this methodology.

The new model system with the EEDPM introduced here has the potential benefit to improve the design and operation of continuous casting systems by better modeling the transport and capture of bubbles and solid particles, which are important for clean steel production. Future publications are planned to describe the components of this model system in detail, in addition to their application to improve continuous casting processes. As future work, the EEDPM model can readily track the transport of additional solid particles as another DPM phase in the model, in addition to gas bubbles, and the advanced capture criteria are readily applicable to their entrapment into the solidifying shell. The model system is still not complete, however. In addition to capture into the shell, it is possible to simulate the attachment of solid particles onto the bubble interfaces by considering the interaction of bubbles and solid particles with proper capture criteria. In addition, the removal of bubbles across the interface between the steel and top slag layers is not automatic and deserves proper modeling treatment. By combining the EEDPM model with other existing models, and improving them, the new system introduced here has the potential to enable future improvements to complex commercial systems involving multiphase turbulent flow of metals, such as steel continuous casting.

CONCLUSION

To solve the challenging issues associated with multiphase flow when injecting argon gas into the molten steel during continuous casting, a new methodology is introduced, which integrates together several existing and new models into a coherent system.

- Accurate gas flow rate and initial bubble size entering into the flow system from the UTN wall can be calculated from a porous flow model of the nozzle refractory, a two-step analytical model of initial bubble formation in downward flow, a correlation model of the number of active sites in porous material, and a Rosin–Rammler function for the size distribution.
- The danger of gas aspiration due to negative pressure inside the nozzle can be estimated with a 1D pressure energy model. In addition to estimating the aspirated gas flow rate, this model can also provide the overall pressure distribution for subsequent models.
- The evolution and redistribution of argon gas in the nozzle as gas pockets and/or bubbles through coalescence, breakup, shearing off, and volumetric expansion in the complex nozzle geometry can be simulated with a new hybrid model, EEDPM. The new model has been systematically validated through three test problems and then applied to simulate the formation of gas pockets and bubble size distributions in a molten-metal/argon gas system.
- With the help of an advanced capture criterion, and the bubble size distribution from the EEDPM model, the flow pattern, transport, and entrapment of gas bubbles into the continuous-cast strand can be better estimated with this new modeling methodology.

ACKNOWLEDGEMENTS

The authors are thankful for support from the Continuous Casting Consortium at the University of Illinois at Urbana-Champaign and the US National Science Foundation (Grant CMMI 15-63553).

REFERENCES

1. G.C. Duderstadt, R.K. Iyengar, and J.M. Matesa, *JOM* 20, 89 (1968).
2. H. Bai and B.G. Thomas, *Metall. Trans. B* 32, 707 (2001).
3. L. Zhang and S. Taniguchi, *Int. Mater. Rev.* 45, 59 (2000).
4. R. Liu and B.G. Thomas, *Metall. Trans. B* 46, 388 (2015).
5. K. Timmel, N. Shevchenko, M. Röder, M. Anderhuber, P. Gardin, S. Eckert, and G. Gerbeth, *Metall. Trans. B* 46, 700 (2015).
6. Z.Q. Liu, F.S. Qi, B.K. Li, and S.C.P. Cheung, *Int. J. Multiph. Flow* 79, 190 (2016).
7. L.C. Hibbeler and B.G. Thomas, *Iron Steel Technol.* 10, 121 (2013).
8. K. Jin, S.P. Vanka, and B.G. Thomas, *Metall. Trans. B* 46, 933 (2018).
9. L. Zhang, *JOM* 65, 1138 (2013).
10. H. Bai and B.G. Thomas, *Metall. Trans. B* 32, 1143 (2001).
11. S.M. Cho, B.G. Thomas, and S.H. Kim, University of Illinois, Urbana, unpublished research (2018).
12. G.G. Lee, B.G. Thomas, and S.H. Kim, *Met. Mater. Int.* 16, 501 (2010).
13. K. Jin, B.G. Thomas, and X. Ruan, *Metall. Mater. Trans. B* 47, 548 (2016).
14. R. Liu, Ph.D. thesis, University of Illinois, Urbana (2014).
15. H. Yang, Ph.D. thesis, University of Illinois, Urbana (2018).
16. H. Yang and B.G. Thomas, in *SteelSIM 2017*, (Qingdao, China, 2017).
17. H. Yang, S.P. Vanka, and B.G. Thomas, in *TMS Annual Meeting and Exhibition*, (Springer, 2018), pp. 119–131.
18. F.H. Harlow and A.A. Amsden, *J. Comput. Phys.* 17, 19 (1975).
19. J.J. Riley, *Phys. Fluids* 17, 292 (1974).
20. H. Yang, S.P. Vanka, and B.G. Thomas, *J. Fluids Eng.* 58, 201 (2018).
21. A. Tomiyama, I. Kataoka, I. Zun, and T. Sakaguchi, *JSME Int. J. Ser. B* 41, 472 (1998).
22. K. Jin, P. Kumar, S.P. Vanka, and B.G. Thomas, *Phys. Fluids* 28, 093301 (2016).
23. Z. Liu, L. Li, F. Qi, B. Li, M. Jiang, and F. Tsukihashi, *Metall. Mater. Trans. B* 46, 406 (2015).
24. Z. Liu, F. Qi, B. Li, and M. Jiang, *Metall. Mater. Trans. B* 46, 933 (2015).
25. R. Chaudhary, B.G. Thomas, and S.P. Vanka, *Metall. Mater. Trans. B* 43, 532 (2012).
26. S.M. Cho, S.H. Kim, and B.G. Thomas, *ISIJ Int.* 54, 845 (2014).
27. S.M. Cho, S.H. Kim, and B.G. Thomas, *ISIJ Int.* 54, 855 (2014).

28. Y.-S. Hwang, P.-R. Cha, H.-S. Nam, K.-H. Moon, and J.-K. Yoon, *ISIJ Int.* 37, 659 (1997).
29. B. Li, T. Okane, and T. Umeda, *Metall. Mater. Trans. B* 31, 1491 (2000).
30. T. Toh, H. Hasegawa, and H. Harada, *ISIJ Int.* 41, 1245 (2001).
31. H. Yu and M. Zhu, *ISIJ Int.* 48, 584 (2008).
32. H. Bai and B.G. Thomas, *Metall. Mater. Trans. B* 32, 269 (2001).
33. L. Zhang, Y. Wang, and X. Zuo, *Metall. Mater. Trans. B* 39, 534 (2008).
34. B.G. Thomas, Q. Yuan, S. Mahmood, R. Liu, and R. Chaudhary, *Metall. Mater. Trans. B* 45, 22 (2014).
35. Q. Yuan, B.G. Thomas, and S. Vanka, *Metall. Mater. Trans. B* 35, 685 (2004).
36. Q. Yuan, B.G. Thomas, and S.P. Vanka, *Metall. Mater. Trans. B* 35, 703 (2004).
37. J.W. Garvin, Y. Yang, and H.S. Udaykumar, *Int. J. Heat Mass Transf.* 50, 2969 (2007).
38. A.V. Catalina, S. Mukherjee, and D.M. Stefanescu, *Metall. Mater. Trans. A* 31, 2559 (2000).
39. L.F. Zhang and Y.F. Wang, *JOM* 64, 1063 (2012).
40. K. Jin and B.G. Thomas, University of Illinois, Urbana, IL, CCC Annual Meeting, August 19, 2015, pp. 1–12.